Spectroscopic Characterization of Matrix-Isolated Phenylcarbene and Cycloheptatetraene†

Stephan Matzinger and Thomas Bally*

Institut de Chimie Physique, Université de Fribourg, Pérolles, CH-1700 Fribourg, Switzerland

Received: September 30, 1999; In Final Form: November 30, 1999

The full UV/VIS and IR spectra are presented for phenylmethylene (**1**) and its rearrangement product, cycloheptatetraene (**2**). The spectra are assigned and discussed on the basis of CASSCF/CASPT2 excited-state and of scaled B3LYP force-field calculations, respectively. The optical spectrum of **1** is very similar in appearance to that of the iso-π-electronic benzyl radical, which demonstrates that the unpaired σ-electron does not interfere noticeably with the π-electronic structure. The IR spectrum of **1** is not very well reproduced by the unscaled B3LYP calculations because of pronounced anharmonicity of the Ph−C−H bending mode, and even a differentiated scaling of the harmonic force field cannot fully remedy this. In contrast, the IR spectrum of **2** is very well reproduced and the corresponding valence force field shows the expected properties for this cyclic allene.

1. Introduction

Nearly 40 years have passed since the classical experiments of Trozzolo et al. led to the identification of phenylcarbene (**1**) as a ground-state triplet species by electron spin resonance (ESR) spectroscopy.[1] At that time, the question of whether triplet carbenes are linear or bent had not been definitively answered,[2] but experiments on ^{13}C-labeled **1** soon settled this question in favor of a bent structure.[3] Subsequently, several groups provided independent evidence that **1** rearranges to a ring-expanded product that, in the absence of trapping agents, dimerizes to heptafulvene.[4−6] In the presence of electron-deficient olefins, spirononatetraenes were formed.[7] Hence this rearrangement product was assigned to cycloheptatrienylidene (presumably in its singlet state because of the aromatic 6π electron system associated with this electronic structure[8]) on the basis also of the results of trapping studies.

In the 1980s this assignment was challenged by the group of Chapman who showed that the rearrangement of **1**, generated in low-temperature matrices, can also be induced photochemically.[9] However, the product obtained in this way failed to yield the expected ketene on annealing in CO-containing matrices, that is, the characteristic signature of singlet carbenes (because it showed no ESR signal, the triplet state of cycloheptatrienylidene could likewise be ruled out). On the other hand, IR bands around 1815 cm^{-1}, which were only slightly shifted on deuteration, indicated the presence of a bent allenic moiety such as it would be expected if the cyclic product obtained from **1** has the cycloheptatetraene structure, **2**. These findings were later substantiated in a comprehensive study using different precursors and isotopomers.[10]

More recently, the intricacies of the potential energy surfaces linking **1** and **2** have been sorted out in great detail by high-level ab initio calculations[11−13] that also confirmed the assignment of the IR spectrum observed by Chapman and colleagues and attributed to **2**.[11] However, in view of the amount and detail of attention that this problem has recently received on the theoretical side, it is surprising that neither **1** nor **2** were ever subjected to a complete characterization by UV/VIS or IR spectroscopy. It is the purpose of this study to fill this gap by presenting for the first time complete electronic absorption (EA) and IR spectra of the two compounds, together with assignments based on ab initio and scaled force-field calculations. We will use this as a starting point in a study of the corresponding radical cations.[14]

2. Methods

2.1. Syntheses. Phenyldiazomethane (PDM) was prepared according to the standard procedure of Creary.[15] The deuterated derivatives were made according to the same procedure from appropriately deuterated benzaldehydes. Benzaldehyde-d_1 was obtained by cyanide-induced cleavage of benzil in the presence of D_2O.[16] Benzil (13.2 g) was suspended in 30 mL of dry dioxane with 12 mL of D_2O. NaCN (3.6 g) was added in four batches and the resulting yellow suspension was stirred for 20 min, leading to the formation of a precipitate. After adding 120 mL of water, the reaction mixture was extracted three times with 50 mL of diethyl ether, which, after washing, drying, and evaporation yielded a yellow liquid. After careful distillation, benzaldehyde-d_1 was obtained in 20% yield.

Benzaldehyde-d_6 was prepared by cerium ammonium nitrate oxidation of toluene-d_8 in 50% acetic acid at 90 °C. After extraction with ether and workup, the desired product was obtained in 50% yield. Although the benzaldehydes obtained in this manner were isotopically pure (>99%) by gas chromatography−mass spectrometry, 25% of the deuterium atoms attached to the diazo group in PDM had exchanged, presumably during the formation of the tosylhydrazone salt.[10] However, this did not prove to be a serious problem in the identification of the important bands of deuterated **1** and **2**.

2.2. Sample Preparation. A mixture of 1 part of carefully purified PDM in 1000 parts of argon (mixed sometimes with 10−20% N_2 to improve the optical properties of the matrix) was slowly deposited on a CsI plate at 20 K. To prevent photolysis of the incipient **1**,[17] deazotation of PDM was effected by irradiation with an Ar ion laser whose emission lines at 485−515 nm coincide well with the very weak n→π* band of PDM (λ_{max} = 490 nm). To prevent destruction of the matrix, the laser

* Author for correspondence.
† Part of the special issue "Marilyn Jacox Festschrift".

10.1021/jp993496j CCC: $19.00
Published on Web 02/02/2000

power had to be reduced to 2.5 W and the beam had to be defocussed to a diameter of 8 mm. Under these conditions, it took about 5 h to achieve >99.5% deazotation of PDM, as judged by its intense 2066 cm^{-1} IR band. Under these conditions no conversion of **1** to **2** was observed. This rearrangement was induced by subsequent irradiation at >420 nm.

2.3. Instrumental. Electronic absorption (EA) spectra were measured on a Perkin-Elmer Lambda-19 spectrometer (200−2000 nm). IR spectra were measured on a Bomem DA3 interferometer (4000−500 cm^{-1} with a mercury−cadmium−telluride detector, 600−200 cm^{-1} with a He-cooled Si bolometer.

2.4. Quantum Chemical Calculations. The B3LYP/6-31G* geometries and Cartesian second derivatives of **1** and **2** were taken from our previous theoretical study.[11] Excited-state energies were calculated at the same geometries by the CASPT2 procedure[18] with the ANO-S basis set of Pierloot et al.[19] using the MOLCAS program.[20] The active spaces used in these calculations are described in the Tables.

2.5. Scaled Force-Field Calculations. On the basis of the available spectroscopic data, the B3LYP/6-31G* force fields were refined according to the method of Pulay et al.[21] For this purpose, the Cartesian force fields from the Gaussian calculations were transformed into sets of nonredundant symmetry-adapted valence coordinates S_1-S_{33}, assembled from corresponding sets of local valence coordinates R_1-R_{33} (in the case of **1** the local valence coordinates are already symmetry-adapted, so no further transformation is necessary). These coordinates were grouped into different classes (principally C−H, C−C, and C═C stretches, in-plane and out-of-plane ring deformations, C−H rocking, and C−H wagging, sometimes divided into subclasses), whereupon a separate scaling factor was assigned to the diagonal force constants for each class. According to the Pulay procedure,[21] the off-diagonal force constants are scaled by the geometric mean of the constants found for the corresponding diagonal elements.

Using a program developed earlier in our group,[22] the scaling constants were then optimized by minimizing the root mean-square difference between calculated and observed fundamental frequencies by means of a Simplex algorithm. Thereby, great care has to be taken to assure correct assignments of the IR bands.[23] This was effected by first scaling the force fields with few scaling factors, using only the most intense and most unambiguously assignable IR bands, and then proceeding to a refinement by introducing progressively more scaling factors and taking into account smaller bands in the spectra as their assignment became clear from the force field. This procedure eventually allowed us also to distinguish quite clearly between fundamentals and combination bands in the case of **1**.

3. Results and Discussion

3.1. Optical Spectra, Excited-State Electronic Structure. After >99% photolysis of PDM-d_0 at 480−515 nm a difference spectrum was obtained whose blue to near-UV part is shown in Figure 1a. It shows great similarity to that published by West et al. in 1982,[9] except that the features between 380 and 360 nm are more intense. Indeed, one can show by successive irradiation of this sample with a medium-pressure Hg lamp through a 365-nm interference filter (difference spectrum 1b), and then with a 420-nm cutoff filter (spectrum 1c), that the near-UV group of bands (which had been observed similarly by West et al. upon photolysis of PDM) is actually the sum of the spectra of *two species*.

The result of the first bleaching at 365 nm is a partial reformation of PDM, which suggests that the species absorbing

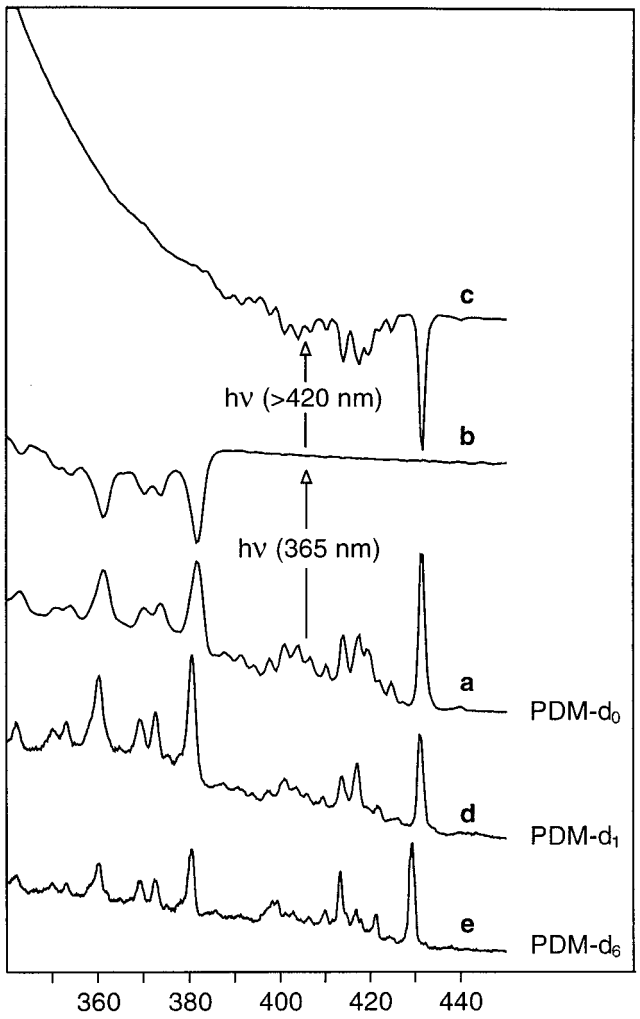

Figure 1. (a) Spectrum obtained after complete photodeazotation of phenyldiazomethane (PDM) in Ar at 12 K by irradiation with an argon ion laser at 480−520 nm (multimode) for 5 h; (b) difference spectrum for the irradiation of the sample giving spectrum (a) at 365 nm [bleaching of phenyldiazirine (PD), see text]; (c) difference spectrum for the bleaching of **1** at >420 nm; (d),(e) spectra obtained analogously to (a) with deuterated PDM.

at 380−340 nm is an isomer of PDM. Comparison with an authentic matrix-isolated sample[24] shows that it is in fact phenyldiazirine (PD). Hence, the conclusion of West et al.[9] that no PD is formed on photolysis of PDM is not completely correct, although the ratio of photoisomerization to cleavage is quite small. The >420-nm irradiation leads to the disappearance of the sharp group of peaks at 430−380 nm, which we attributed to a bleaching of **1** that is accompanied by the increase of a more intense, broad absorption tailing out to about 400 nm (Figure 1c). Note also that deuteration of the sample (Figure 1d and e) leaves the spectrum of PD almost unaffected, whereas it results in significant changes of the vibronic structure of the absorptions due to **1**.

By working with three samples of different concentration, all treated according to the above protocol, we were able to assemble a full spectrum of **1** that is displayed in the upper part of Figure 2, along with a schematic rendition of the the CASPT2 predictions that will be discussed below. These results show that the the sharp peaks at 430−380 nm (2.88−3.25 eV) comprise in fact *two* excited states (which we will not attempt to distinguish, see below), whereas the bands with origins at 300 nm (4.13 eV) and 246 nm (5.04 eV) arise from transitions

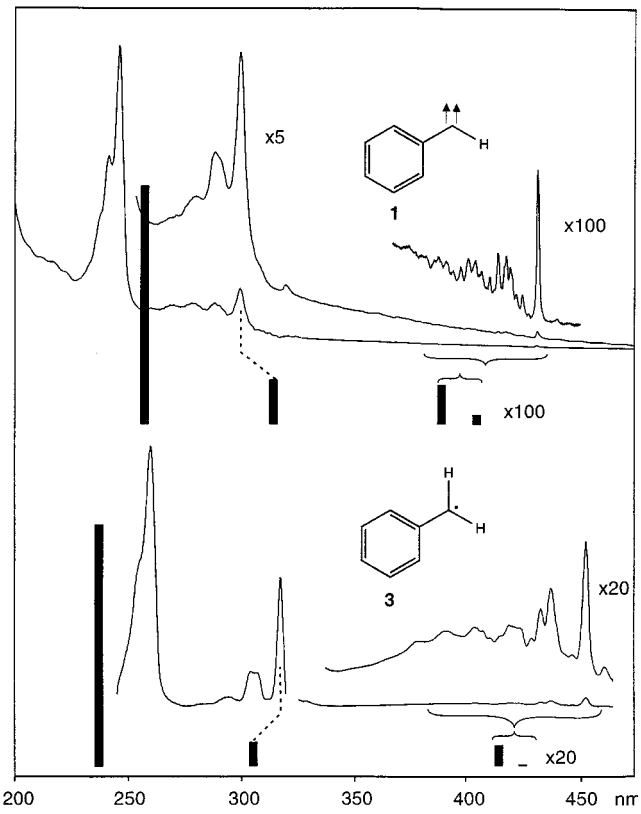

Figure 2. Top: complete UV/VIS absorption spectrum of **1** obtained by photolysis of Ar matrices containing different amounts of PDM; bottom: excitation spectrum of **3**, replotted from the literature.[25] The black bars are electronic transitions predicted by CASPT2 (see Tables 1 and 2 for corresponding numbers).

to the next higher excited states of the same symmetry as the two close-lying ones around 3 eV.

Also shown in Figure 2 (bottom) is the spectrum of the iso-π electronic analogue of **1**, the benzyl radical **3** (excitation spectra in 3-methylpentane at 77 K[25]). This spectrum has a very similar appearance to that of **1**, which indicates that there is some analogy in the electronic structure of the two compounds.[26] The π-electronic structure of both compounds as it expresses itself in the UV/VIS spectra can be adequately described by two pairs of excited configurations arising through $\pi_3 \rightarrow \pi_4/\pi_4 \rightarrow \pi_5^*$ and $\pi_2 \rightarrow \pi_4/\pi_4 \rightarrow \pi_6^*$ electron promotion denoted as a/b and c/d in Figure 3. Both pairs of configurations, which are degenerate at a Hückel π-molecular orbital (MO) level (although they are of opposite symmetry in **3**), interact among themselves to form positive and negative linear combinations. The resulting states corresponding to the two *negative* combinations happen to be again nearly degenerate,[27] whereas the two higher-lying *positive* combinations are well separated in energy. The transition moments for the above pairs of electron promotions, a/b and c/d, are of very similar magnitude and direction, that is, they tend to cancel in the negative combinations but reinforce each other in the positive one. Consequently, the two lower-energy transitions are associated with very weak oscillator strengths, whereas those in the UV are much more intense.

The above qualitative features of the electronic structures of **1** and **3** are very clearly borne out by the CASPT2 calculations shown in Tables 1 and 2, respectively. An interesting feature of these results is that the state arising by positive combination of excitations c and d lies very high at the CASSF level (it is the 11th excited state of A″ symmetry in **1**, and the fifth excited state of B_1 symmetry in **3**) and is depressed by an unusually large amount by dynamic correlation (2.6 eV in **1**, 1.3 eV in **3**)

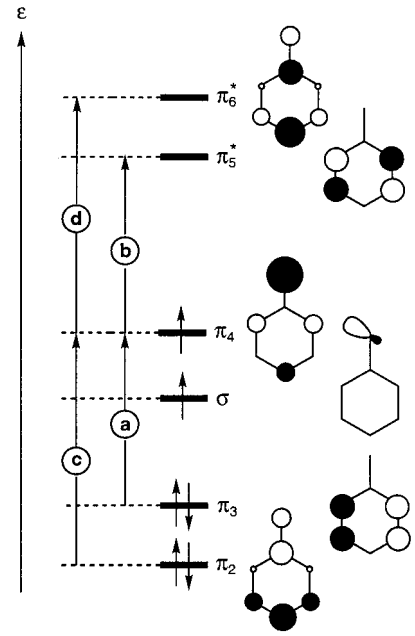

Figure 3. Molecular orbitals (MOs) and excitations a−d that are important in discussing the excited-state electronic structure of **1** and **3** (the σ-MO in the center exists only for **1**).

TABLE 1: Excited States of Phenylmethylene (1) According to CASPT2 Calculations

states	EAS (eV)	CASSCF[a] (eV)	CASPT2[b] (eV)	CASPT2[b] (*f*)[d]	major configurations[c]
$1^2A''$	(0)	(0)		(0)	82% ground config.
$2^2A''$	2.88	3.17	3.15	0.0004	39% c−32% d
$3^2A''$	(2.95)	3.29	3.03	0.0001	36% a−33% b
$4^2A''$		4.60	4.48	0.0001	70% $\pi_3 \rightarrow \pi_5^*$
$5^2A''$		5.44	5.16	0.0001	42% $\pi_3 \rightarrow \pi_5^*$ +16% $\pi_1 \rightarrow \pi_4$
$6^2A''$		5.77	5.44	$<10^{-4}$	34% $\pi_2 \rightarrow \pi_5^*$ −27% $\pi_3 \rightarrow \pi_6^*$
$7^2A''$	4.13	6.21	3.91	0.0445	39% a + 41% b
$8^2A''$		6.43	6.05	0.0005	22% $\pi_2 \rightarrow \pi_5^*$ + others
$9^2A''$		6.67	6.19	0.0001	(highly mixed)
$10^2A''$		6.91	6.23	0.0002	35% $\pi_2 \rightarrow \pi_5^*$ + others
$11^2A''$	5.04	7.45	4.79	0.2389	34% c + 39% d
$1^2A'$	(≈4 eV)	4.11	4.13	0.0004	69% $\pi_2 \rightarrow \sigma$
$2^2A'$		4.91	4.29	$<10^{-4}$	75% $\pi_3 \rightarrow \sigma$
$3^2A'$		5.58	5.30	$<10^{-4}$	70% $\pi_3 \rightarrow \sigma$ + $\pi_4 \rightarrow \pi_5^*$

[a] The active space comprises eight electrons in seven π-MOs and one σ-MO; state averaging was done over the first 11 A″ states and on the first 5 A′ states, respectively. States are ordered according to CASSCF energies within each symmetry. [b] Calculated with a level shift of 0.3 au for the A″-states and 0.2 au for the A′-states. [c] cf. Figure 3 for MOs and excitations a−d. [d] Oscillator strength for electronic transition, based on the CASSCF wave functions and the CASPT2 energy differences.

to become the fifth π-excited state (in both compounds a weak transition is predicted to occur to a lower-lying state that corresponds essentially to $\pi_3 \rightarrow \pi_5^*$ excitations). Although the CASPT2 excitation energies are generally within 0.25 eV of the observed peak positions, it is a bit disappointing that this rather sophisticated level of theory is unable to predict the shifts of the higher excited states between **1** and **3** correctly.[28]

The strong similarity of the optical spectra of **1** and **3** raises the question of whether and how the unpaired σ-electron, which distinguishes **1** from **3**, expresses its presence in the spectrum

TABLE 2: Excited States of Benzyl Radical (B•) According to CASPT2 Calculations

states	EAS (eV)	CASSCF[a] (eV)	CASPT2 (eV)	CASPT2 (*f*)[c]	major configurations[b]
1^2B_1	(0)	(0)		(0)	83% ground config.
2^2B_1	2.73	3.01	2.96	0.0021	44% c−33% d
3^2B_1		4.98	4.72	0.0004	58% $\pi_3 \rightarrow \pi_5^*$ +12% $\pi_1 \rightarrow \pi_4$
4^2B_1		6.24	5.85	0.0001	24% $\pi_1 \rightarrow \pi_4$ + others
5^2B_1	4.77	5.44	5.21	0.4826	34% c + 41% d
1^2A_2	(2.94)	3.08	2.88	0.0001	29% a−35% b
2^2A_2	3.90	5.47	4.03	0.0488	99% a + 43% b
3^2A_2		5.94	5.57	0.0067	70% $\pi_3 \rightarrow \sigma + \pi_4 \rightarrow \pi_5^*$

[a] The active space comprises seven electrons in seven b_1 and three a_2 π-MOs; state averaging was done over the first five $^2B_1$ and on the first three $^2A_2$ states, respectively. States are ordered according to CASSCF energies within each symmetry. [b] cf. Figure 3 for MOs and excitations a−d. [c] Oscillator strength for electronic transition, based on the CASSCF wave functions and the CASPT2 energy differences.

of **1**. According to the CASPT2 calculations reported in Table 1 (A′ states), excitations involving $\pi \rightarrow \sigma$ electron promotion should indeed occur in the range of observation of our experiment (the first five $^2A'$ excited states involve no $\sigma-\pi^*$ excitation). The first of the corresponding transitions is predicted at 300 nm, with an oscillator strength commensurate with that of the stronger of the two visible transitions. It could be that this $\pi_2 \rightarrow \sigma$ excitation is responsible for the low-energy shoulder to the strong 300-nm band that was observed in all experiments (contrary to the peak at ≈320 nm, which must be due to an impurity). The next few $\pi \rightarrow \sigma$ transitions are, however, predicted to be too weak to be observed next to the strong excitations within the π-MOs. Thus, the presence of the unpaired in-plane σ-electron does not seem to manifest itself in any clearly palpable way in the spectrum of **1**, in stark contrast to the corresponding radical cation, $\mathbf{1}^{\bullet+}$, which is iso-π-electronic to benzyl cation, but whose spectrum shows no similarity whatsoever to that of the latter.[14]

Finally, we wish to comment on the apparent discrepancy between the ordering of the first two states of **1** as predicted by CASPT2 and the vibronic pattern of the first EA band: as in the case of **3**,[29] the two near-degenerate states of **1** are expected to be strongly coupled by vibronic interaction; hence any assignment of individual peaks to one of the other of these states is probably futile. In **3** the coupling of the two states seems to occur primarily through ν_{8b} and ν_{6b}, which are vibrations of the benzene ring (and much less so by the appropriate vibrations of the CH_2 group).[30] If this is the also the case in **1** we expect that deuteration of the carbene center will affect the spectrum to a much lesser extent than deuteration of the benzene ring, an expectation that is confirmed by experiment (cf. Figure 1c−e).

Bleaching of the very photosensitive **1** is thought to lead exclusively to ring expansion, resulting in the formation of cycloheptatetraene, **2**. We will confirm this conjecture below by IR spectroscopy, but first examine the changes in the optical spectra. As shown already by McMahon et al.,[10] the EA spectrum that remains after full bleaching of **1** is quite nondescript, consisting of a broad and nearly featureless band whose peak falls outside the observation range and which tails all the way out to 400 nm (cf. difference spectrum 1c). CASPT2 calculation on **2** (see Table S7 in the Supporting Information) predict indeed that no absorption bands are expected to peak above 340 nm where a weak transition corresponding essentially to highest occupied MO → lowest unoccupied MO excitation is predicted to occur. Apparently this band tails out to 400 nm, which could indicate a strong geometry change in the corresponding excited state.

3.2. IR Spectra. As mentioned above, deazotation of PDM at 480−520 nm leads mainly to formation of **1** plus a small amount of PD, which can be bleached efficiently without affecting **1** by short irradiation at 365 nm. This finding is confirmed by the IR spectra recorded in tandem with the EA spectra shown in Figure 1. However, the most telling set of vibrational spectra is obtained on bleaching of **1** at >420 nm. A difference IR spectrum for this process is shown in Figure 4, along with the predictions from B3LYP/6-31G* calculations (frequencies scaled by a single factor of 0.95).

It is immediately evident that the IR bands that arise in this process match very well with the B3LYP predictions for **2**, perhaps apart from the relative intensities of the pair of peaks at 1364 and 1380 cm^{-1}, which are found to be much more disparate than predicted. Also, the bands at 404 and 1823 cm^{-1} are split into pairs, presumably due to the operation of a matrix site effect (note that the pair of peaks around 675 cm^{-1} is due to *two* transitions that happen to coincide in the calculated spectrum). Similarly good matches are found for **2**-d_1 and **2**-d_6 (see Supporting Information). From a fit to the spectra of the protio- and the perdeutero-isotopomer to a scaled B3LYP force field we obtained the force field described in the following section, which reproduced the experimental frequencies of all three isotopomers with a root mean-square deviation of less than 4 cm^{-1}, which instills substantial confidence in the assignment of the spectra to the cyclic allene, **2**. Most importantly, only very few and small IR bands could not be attributed to **2**, which confirms that this is the only—or, at least, the very major—product of the bleaching of **1**.

The situation is more complicated in the case of the IR bands which decrease in the bleaching process and which, in view of the above-described clean formation of **2**, would therefore have to be attributed exclusively to **1**. However, before going into any detail, we wish to point out that most of the important features of the experimental spectrum, in particular the three intense bands at 443, 670, and 741 cm^{-1}, and most of the prominent peaks between 1000 and 1600 cm^{-1}, are similarly well reproduced by the B3LYP calculations as in the case of **2**. However, between 800 and 1000 cm^{-1} the agreement between observed and calculated spectra leaves much to be desired, and a closer inspection of the region from there up to 1600 cm^{-1} also reveals a number of bands that cannot be attributed to fundamentals of **1**, although they appeared reproducibly in all experiments. Similar discrepancies were noted in the case of **1**-d_6, whereas, interestingly, the matching was considerably better in **1**-d_1 (see Supporting Information).

Let us first address the problem of the blatant mismatch of experiment and theory in the region of 800−1000 cm^{-1} where the experimental spectrum shows only a number of weak bands, whereas B3LYP predicts an intense band at 872 cm^{-1}. Inspection of the corresponding normal mode shows that it corresponds in large part to the Ph−C−H bending coordinate. It is known that the bending potential of $^3CH_2$ is quite anharmonic ($\omega_e x_e$ for the bending vibration is 58.5 cm^{-1})[31] and there is no reason why this should be very different in **1**. Indeed, B3LYP calculations of this potential (see Figure 5) reveal a rather pronounced deviation from a "harmonic" parabolic shape (cf. dashed line).[32]

Thus it is clear that the harmonic approximation at the basis of the B3LYP force field is bound to fail for this particular deformation. Solving the one-dimensional vibrational Schrödinger equation for a harmonic potential fitted to the region

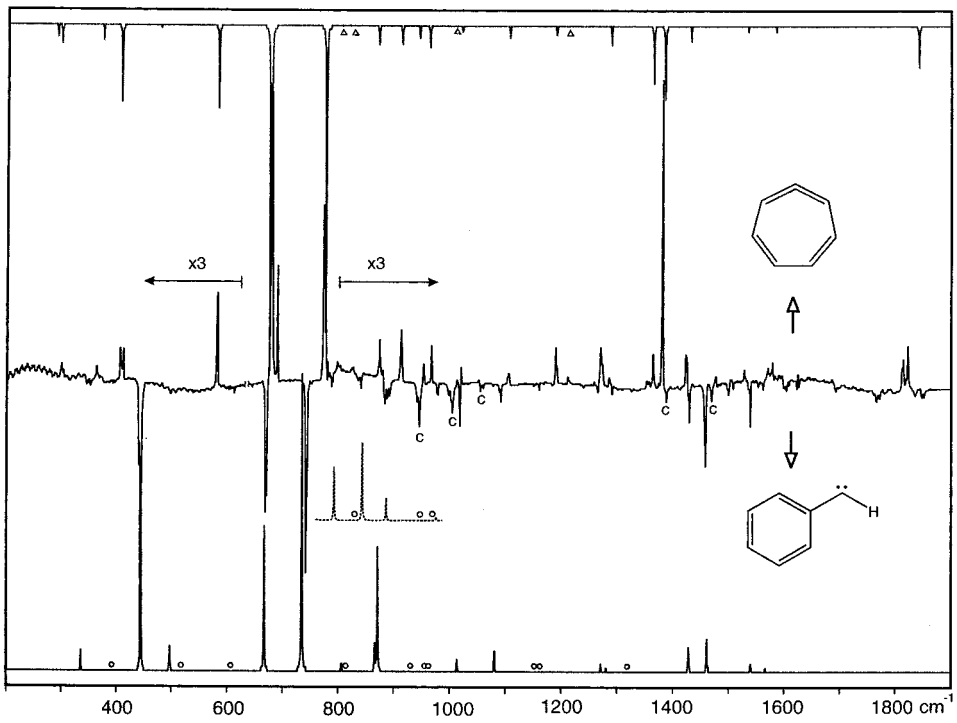

Figure 4. IR difference spectrum for the bleaching of **1** and the concomitant formation of **2** by irradiation at >420 nm. The spectra at the top and the bottom are graphical representations of B3LYP/6-31G* predictions (all frequencies scaled by 0.95). The circles (**1**) and triangles (**2**) indicate positions of bands that are too weak to show up in the traces. The dashed inset line shows the result of re-fitting the spectrum with a separate scaling factor for the Ph−C−H bending coordinate (see text).

TABLE 3: Definition of Valence Coordinates for 2

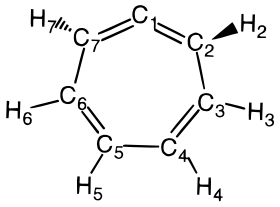

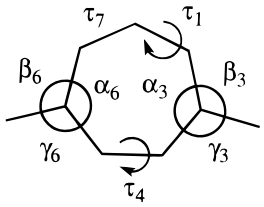

no.	description	no.	description
R_1	C_1-C_7 stretch	R_{14}	C_7-H_7 rock $= \Delta\beta_7-\Delta\gamma_7$
R_2	C_1-C_2 stretch	R_{15}	C_2-H_2 rock $= \Delta\beta_2-\Delta\gamma_2$
R_3	C_7-C_6 stretch	R_{16}	C_6-H_6 rock $= \Delta\beta_6-\Delta\gamma_6$
R_4	C_2-C_3 stretch	R_{17}	C_3-H_3 rock $= \Delta\beta_3-\Delta\gamma_3$
R_5	C_5-C_6 stretch	R_{18}	C_5-H_5 rock $= \Delta\beta_5-\Delta\gamma_5$
R_6	C_4-C_3 stretch	R_{19}	C_4-H_4 rock $= \Delta\beta_4-\Delta\gamma_4$
R_7	C_4-C_5 stretch	R_{20}	H_7 wag out of (C_1, C_7, C_6) plane
R_8	C_7-H_7 stretch	R_{21}	H_2 wag out of (C_1, C_2, C_3) plane
R_9	C_2-H_2 stretch	R_{22}	H_6 wag out of (C_5, C_6, C_7) plane
R_{10}	C_6-H_6 stretch	R_{23}	H_3 wag out of (C_2, C_3, C_4) plane
R_{11}	C_3-H_3 stretch	R_{24}	H_5 wag out of (C_4, C_5, C_6) plane
R_{12}	C_5-H_5 stretch	R_{25}	H_4 wag out of (C_3, C_4, C_5) plane
R_{13}	C_4-H_4 stretch		

$R_{26}^{a,b} = \Delta\alpha_1 + b(\Delta\alpha_2 + \Delta\alpha_7) + c(\Delta\alpha_3 + \Delta\alpha_6) + a(\Delta\alpha_4 + \Delta\alpha_5)$
$R_{27}^{a,b} = \Delta\alpha_1 + c(\Delta\alpha_2 + \Delta\alpha_7) + a(\Delta\alpha_3 + \Delta\alpha_6) + b(\Delta\alpha_4 + \Delta\alpha_5)$
$R_{28}^{a,b} = f(\Delta\alpha_2 - \Delta\alpha_7) + d(\Delta\alpha_6 - \Delta\alpha_3) + e(\Delta\alpha_4 - \Delta\alpha_5)$
$R_{29}^{a,b} = e(\Delta\alpha_7 - \Delta\alpha_2) + f(\Delta\alpha_3 - \Delta\alpha_6) + d(\Delta\alpha_4 - \Delta\alpha_5)$
$R_{30}^{a,c} = a(\Delta\tau_1 + \Delta\tau_7) + c(\Delta\tau_2 + \Delta\tau_6) + b(\Delta\tau_3 + \Delta\tau_5) + \tau_4$
$R_{31}^{a,c} = b(\Delta\tau_1 + \Delta\tau_7) + a(\Delta\tau_2 + \Delta\tau_6) + c(\Delta\tau_3 + \Delta\tau_5) + \tau_4$
$R_{32}^{a,c} = d(\Delta\tau_1 - \Delta\tau_7) + f(\Delta\tau_2 - \Delta\tau_6) + e(\Delta\tau_5 - \Delta\tau_3)$
$R_{33}^{a,c} = e(\Delta\tau_7 - \Delta\tau_1) + d(\Delta\tau_2 - \Delta\tau_6) + f(\Delta\tau_5 - \Delta\tau_3)$

[a] $\alpha = 360°/7$; $a = \cos(\alpha)$; $b = \cos(2\alpha)$; $c = \cos(3\alpha)$, $d = \sin(\alpha)$, $e = \sin(2\alpha)$; $f = \sin(3\alpha)$. [b] Ring deformation. [c] Ring torsion.

around the potential energy minimum (±10°)[33] resulted in a spacing of the vibrational levels of 842 cm^{-1}, in good accord with that of the normal mode of **1** which is dominated by this bending coordinate. The same treatment applied to the full,

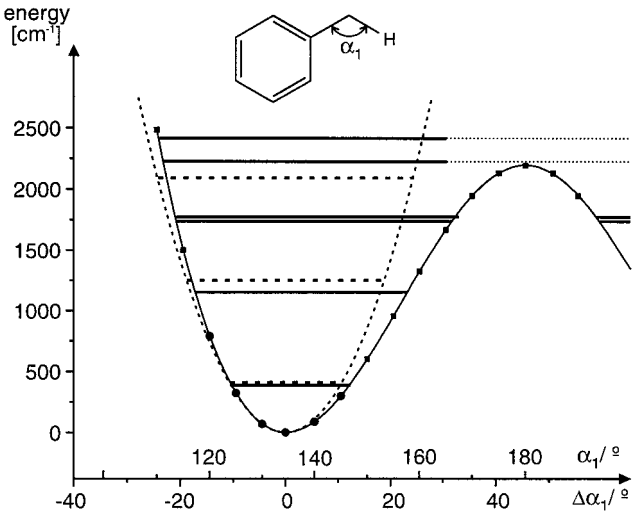

Figure 5. B3LYP/6-31G* potential energy surface for the Ph−C−H bending deformation of **1** (anharmonic potential[33] fitted through squares). Dashed line: harmonic potential fitted to the potential energy points indicated by filled circles.[33] Horizontal lines indicate vibrational energy levels obtained by solving the one-dimensional vibrational Schrödinger equation for the full or the harmonic potential, respectively.

anharmonic potential[33] resulted in an energy difference of 752 cm^{-1} between the lowest two energy levels, which translates into an anharmonicity correction of $\omega_e x_e = 45$ cm^{-1}.

This pronounced anharmonicity of the Ph−C−H bending vibration is clearly at the origin of the mismatch between experiment and theory in the region around 900 cm^{-1}. In view of the predicted anharmonic "bending frequency" of 752 cm^{-1} it would appear tempting to claim that this vibration happens to coincide with the strongest band in the IR spectrum of **1** at 741 cm^{-1}. However, such simple reasoning does not take into account that changing the force constant for Ph−C−H bending

TABLE 4: Symmetry Coordinates for 2 (in C_2 Symmetry)[a]

irrep	no.		definition	no.		definition	no.		definition
A	S_1	=	$R_1 + R_2$	S_2	=	$R_3 + R_4$	S_3	=	$R_5 + R_6$
	S_4	=	R_7	S_5	=	$R_8 + R_9$	S_6	=	$R_{10} + R_{11}$
	S_7	=	$R_{12} + R_{13}$	S_8	=	$R_8 + R_9$	S_9	=	$R_{16} + R_{17}$
	S_{10}	=	$R_{18} + R_{19}$	S_{11}	=	$R_{20} + R_{21}$	S_{12}	=	$R_{22} + R_{23}$
	S_{13}	=	$R_{24} + R_{25}$	S_{14}	=	R_{26}	S_{15}	=	R_{27}
	S_{16}	=	R_{30}	S_{17}	=	R_{31}			
B	S_{18}	=	$R_1 - R_2$	S_{19}	=	$R_3 - R_4$	S_{20}	=	$R_5 - R_6$
	S_{21}	=	$R_1 - R_2$	S_{22}	=	$R_{10} - R_{11}$	S_{23}	=	$R_5 - R_6$
	S_{24}	=	$R_{14} - R_{15}$	S_{25}	=	$R_{16} - R_{17}$	S_{26}	=	$R_5 - R_6$
	S_{27}	=	$R_{20} - R_{21}$	S_{28}	=	$R_{22} - R_{23}$	S_{29}	=	$R_{24} - R_{25}$
	S_{30}	=	R_{28}	S_{31}	=	R_{29}	S_{32}	=	R_{32}
	S_{33}	=	R_{33}						

[a] All combinations of two valence coordinates are normalized by $\sqrt{2}$.

TABLE 5: Final Scaling Factors Used for Fitting of the Scaled Quantum Mechanical (SQM) Force Field of 2

factor	opt. value	coordinates	description
f_1[a]	0.9239	S_5-S_7, $S_{21}-S_{23}$	C−H stretches
f_2	0.9211	S_1, S_{18}	allenic C═C stretches
f_3	0.9356	S_2-S_4, S_{19}, S_{20}	all other C−C stretches
f_4	0.9400	S_8, S_{24}	allenic C−H rocking
f_5	0.9331	S_9, S_{10}, S_{25}, S_{26}	all other C−H rocking
f_6	0.9427	$S_{11}-S_{13}$, $S_{27}-S_{29}$	C−H wagging
f_7	0.9557	S_{14}, S_{15}, S_{30}, S_{31}	in-plane ring deform.
f_8	0.9527	S_{16}, S_{17}, S_{32}, S_{33}	ring torsions

[a] This parameter was fixed (not optimized) due to lack of data.

affects the entire force field, in particular also the mixing with other in-plane modes.

Indeed, the scaled force-field calculations described in the following section show that a lowering of this bending force constant results in a pronounced redistribution of valence deformations among normal modes. This affects not only the positions but also the relative intensities of a few of the bands in the 800−1000 cm^{-1} region, as illustrated by the dashed inset line in Figure 4.[34] Unfortunately, the calculation of a full quartic force field is presently still unfeasible for molecules of the size and (lack of) symmetry of **1**, so we have no method to take the effect of this anharmonicity into account in a theoretically satisfactory fashion.

The second problem, that is, the occurrence of more bands than (predicted) normal modes, is easier to deal with in that most of them can readily be associated with combination bands and overtones (labeled c in Figure 4). Several of them seem to borrow intensity from the intense fundamental at 443 cm^{-1}, notably the strong peak at 945 cm^{-1} (≈443 + 497 cm^{-1}) and the weaker ones at 1054 cm^{-1} (≈443 + 612 cm^{-1}) and 1468 cm^{-1} (≈443 + 1018 cm^{-1}). We are at a loss to explain satisfactorily the bands at 997 cm^{-1} (≈2 × 497 cm^{-1} ?) and 1387 cm^{-1} (≈2 × 443 + 497 cm^{-1} ?), but because these bands appeared reproducibly in all experiments, assigning them to an impurity appears to be out of the question.

3.3. Valence Force Fields of 1 and 2. Armed with the IR spectrum shown in Figure 4 and the corresponding ones for the bleaching of **1**-d_1 and **1**-d_6 shown in the Supporting Information, we proceeded to a refinement of the B3LYP/6-31G* force fields of **1** and **2** according to the procedure of Pulay et al.[21] as described in the Methods section. In the case of **2**, a problem consisted in finding a proper set of deformation and

TABLE 6: Frequencies and Intensities of IR Transition of 2-h_6 Calculated on the Basis of the SQM Force Field of 2 Obtained from a Fit over the IR Spectra of h_6 and d_6-Isotopomers[a]

no.	sym	calc.	exp.	Δ	% int.	potential energy distrib.[b]
1	**A**	3046.9	3048	−1.1	23.3	7(74) + 6(18)
2		3036.5			43.0	5(87) + 7(11)
3		3017.7			1.4	6(80) + 7(14)
4		1530.5	1527	3.5	1.5	3(50) + 4(21) + 10(11)
5		1425.8	1422	3.8	4.0	9(45) + 10(27) + 2(13)
6		1359.5	1364	−4.5	13.6	8(38) + 1(24) + 2(18) + 3(12)
7		1209.7	1211	−1.3	0.2	10(55) + 9(33)
8		1101.9	1104	−2.1	3.5	8(42) + 1(24) + 2(14)
9		1010.0	1012	−2.0	0.0	1(28) + 12(22) + 2(21)
10		963.9	966	−2.1	5.5	13(44) + 17(22) + 12(18)
11		912.1	913	−0.9	4.9	4(33) + 3(17) + 12(13) + 16(10)
12		831.3	826	5.3	0.0	12(30) + 13(24) + 4(10)
13		803.8	798	5.8	0.3	11(53) + 16(22) + 2(14)
14		682.0	689	−7.0	26.3	15(60) + 12(16) + 11(8)
15		584.9	581	3.9	20.3	17(48) + 13(16) + 15(16)
16		407.6	404	3.6	18.9	14(64) + 15(15) + 11(8)
17		297.5	302	−4.5	4.4	16(75)
18	**B**	3038.2	3038	0.2	100.0	21(71) + 22(17) + 23(11)
19		3031.8			31.3	23(51) + 21(26) + 22(22)
20		3013.8	3013	0.8	20.7	22(60) + 23(38)
21		1824.4	1823	1.4	10.0	18(93)
22		1581.2	1579	2.2	1.4	20(60) + 26(18)
23		1379.8	1380	−0.2	17.8	26(47) + 25(30) + 19(18)
24		1286.8	1285	1.8	4.2	24(80)
25		1185.9	1189	−3.1	2.4	25(53) + 26(22) + 20(18)
26		1018.6	1019	−0.4	1.5	19(45) + 28(15) + 20(12)
27		946.0	952	−6.0	3.0	29(33) + 28(26) + 30(18)
28		876.0	874	2.0	4.8	30(67) + 19(12)
29		777.6	772	5.6	75.0	27(57) + 28(18) + 29(8)
30		676.3	679	−2.7	83.8	27(33) + 28(28) + 29(24)
31		479.9	482	−2.1	1.0	33(38) + 31(29) + 32(19)
32		373.5	362	11.5	3.7	33(58) + 31(22) + 32(11)
33		290.3	298	−7.7	3.1	32(54) + 29(26) + 31(11)

[a] The force fields for the d_6 and the d_1-isotopomers, together with the spectra on which they are based, are given in the Supporting Information. [b] Contributions of symmetry coordinates S_1-S_{33} (see Table 4) to each normal mode. Only coordinates that contribute >10% are listed.

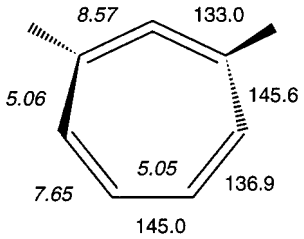

Figure 6. B3LYP/6-31G* C−C bond lengths in pm (normal) and diagonal force constants for C−C stretching in $aJ/Å^2$ (italic) from the scaled force field of **2**.

torsion coordinates for seven-membered rings, because these were not available from the literature. With the help of Prof. Pulay, who kindly supplied the standard weighting factors for the angular and torsional deformations given in the footnote to Table 3, we were finally able to derive the set of valence and symmetry coordinates shown in Tables 3 and 4.

The force field in C_2 symmetry was fitted to the spectra of **2**-d_0 and **2**-d_6, initially with two, then with four, and finally with the eight scaling factors listed in Table 5 (we found that we had to introduce separate scaling factors f_2 and f_4 for the C═C stretching and the C−H rocking coordinates associated with the bent allenic moiety). This resulted in a force field that reproduced all the observed frequencies, including those from the nonsymmetric **2**-d_1, which had not been included in the fitting, with an overall root mean-square deviation of less than 4 cm^{-1} and a maximal deviation of 11.5 cm^{-1} for the ring-puckering mode ν_{32} of **2**-d_0 (see Table 6). All optimized scaling constants (Table 5) lie within the range 0.94 ± 0.02; hence it is not surprising that a single scaling constant of 0.95 had already given a very satisfactory agreement with the experimental spectrum.

The last column of Table 6 presents an analysis of the vibrational structure of **2**-d_0 in terms of the symmetry coordinates in Table 4 (similar tables for the d_1 and the d_6 isotopomers are found in the Supporting Information). It shows that most of the IR bands cannot be associated with individual deformations, with the exception of the antisymmetric allenic stretch at 1823 cm^{-1}, which had already served as the flagpole vibration in the original assignment of **2**.[9] An interesting conclusion that emerges from the analysis of the force field in valence coordinates is that the diagonal elements for the C−C stretches show a clear alternation, in line with the C−C bond length alternation, as shown in Figure 6.

Because of the above-mentioned anharmonicity of the Ph−C−H bending mode, the force-field fitting proved to be more problematic in **1**, although in this case the definition of standard internal coordinates (Table 7) posed no difficulties. Our initial attempt consisted in a separate scaling of the Ph−C−H bending coordinate R_{14} with a factor that was initially taken as the ratio of the square of the anharmonic and harmonic frequencies for this mode calculated above ($752^2/842^2 = 0.798$). This led to a distribution of the contribution of R_{14} (which had constituted 70% of ν_{20} in the unscaled force field) among ν_{19} (61% R_{14}) and ν_{20} (29% R_{14}) and a concomitant change in the contributions of the C−C stretches involving C_1, C_2, and C_7, as well as of the trigonal phenyl ring deformation mode R_{28}.

Although the intensity of the IR transitions corresponding to ν_{19} and ν_{20} was still much too high in comparison to that of the very small peaks in the experimental spectrum, the frequencies were now in much better accord (cf. dashed line in Figure 4). This encouraged us to proceed with a refinement of the force field of **1** on the basis of the spectra of all three isotopomers. Thereby we found that good qualitative accord with the experimental spectra could only be achieved if the C_2-C_1 stretch, rock, and wag were scaled separately, which finally brought the total of the scaling factors up to the 11 shown in Table 8. An analysis of the vibrational structure of **1**-d_0 based on the final optimized force field is presented in the right most column of Table 9. This force field reproduced the IR spectra of all three istopomers, shown in the Supporting information, with an overall root mean-square deviation of 4.4 cm^{-1}.

In contrast to the above case of **2**, the scaling constants show a much larger spread in **1**. Also, the IR transitions involving R_{14} are predicted considerably too intense, that is, the dipole moment derivative for this mode seems to be overestimated by B3LYP. R_{14} involves rehybridization at the carbenic carbon atom, that is, a redistribution of the unpaired σ-electron. The

TABLE 7: Definition of Valence Coordinates for 1[a]

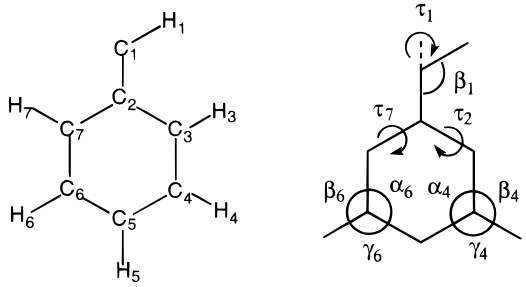

no.	description	no.	description
R_1	C_1-C_2 stretch	R_{14}	$C_2-C_1-H_1$ bend $= \Delta\beta_1$
R_2	C_2-C_3 stretch	R_{15}	C_2-C_1 rock $= \Delta\beta_2-\Delta\gamma_2$
R_3	C_3-C_4 stretch	R_{16}	C_3-H_3 rock $= \Delta\beta_3-\Delta\gamma_3$
R_4	C_4-C_5 stretch	R_{17}	C_7-H_7 rock $= \Delta\beta_7-\Delta\gamma_7$
R_5	C_5-C_6 stretch	R_{18}	C_4-H_4 rock $= \Delta\beta_4-\Delta\gamma_4$
R_6	C_6-C_7 stretch	R_{19}	C_6-H_6 rock $= \Delta\beta_6-\Delta\gamma_6$
R_7	C_7-C_2 stretch	R_{20}	C_5-H_5 rock $= \Delta\beta_5-\Delta\gamma_5$
R_8	C_1-H_1 stretch	R_{21}	C_1-C_2 torsion $= \Delta\tau_1$
R_9	C_3-H_3 stretch	R_{22}	C_1 wag out of (C_2,C_3,C_7) plane
R_{10}	C_7-H_7 stretch	R_{23}	H_3 wag out of (C_2,C_3,C_7) plane
R_{11}	C_4-H_4 stretch	R_{24}	H_7 wag out of (C_2,C_6,C_7) plane
R_{12}	C_6-H_6 stretch	R_{25}	H_4 wag out of (C_3,C_4,C_5) plane
R_{13}	C_5-H_5 stretch	R_{26}	H_6 wag out of (C_5,C_6,C_7) plane
		R_{27}	H_5 wag out of (C_4,C_5,C_6) plane
R_{28}	$= \Delta\alpha_2-\Delta\alpha_3+\Delta\alpha_4-\Delta\alpha_5+\Delta\alpha_6-\Delta\alpha_7$		ring deformation
R_{29}	$= 2\Delta\alpha_2-\Delta\alpha_3-\Delta\alpha_4+2\Delta\alpha_5-\Delta\alpha_6-\Delta\alpha_7$		ring deformation
R_{30}	$= \Delta\alpha_3-\Delta\alpha_4+\Delta\alpha_6-\Delta\alpha_7$		ring deformation
R_{31}	$= \Delta\tau_2-\Delta\tau_3+\Delta\tau_4-\Delta\tau_5+\Delta\tau_6-\Delta\tau_7$		ring puckering
R_{32}	$= \Delta\tau_2-\Delta\tau_4+\Delta\tau_5-\Delta\tau_7$		ring puckering
R_{33}	$= \Delta\tau_2-2\cdot\Delta\tau_3+\Delta\tau_4+\Delta\tau_5-2\cdot\Delta\tau_6+\Delta\tau_7$		ring puckering

[a] Because **1** has only C_s symmetry, no linear combinations of R_1-R_{33} are needed to define symmetry coordinates; coordinates R_1-R_{20} and $R_{28}-R_{30}$ are of a′, $R_{21}-R_{27}$ and $R_{31}-R_{33}$ of a″ symmetry.

TABLE 8: Final Scaling Factors Used for Fitting of SQM Force Field of 1

factor	opt. value	coordinates	description
f_1	0.9638	R_1	C_2-C_1 stretch
f_2	0.9369	R_2-S_7	phenyl C−C stretches
f_3	0.9192[a]	R_8-R_{13}	C−H stretches
f_4	0.8192[b]	R_{14}	Ph−C−H bend
f_5	1.0417	R_{15}	C_2-C_1 rocking
f_6	0.9423	$R_{16}-R_{20}$	phenyl C−H rocking
f_7	0.9832	$R_{28}-R_{30}$	in-plane ring deform.
f_8	0.9581	R_{21}	torsion around C_2-C_1
f_9	0.9113	R_{22}	C_2-C_1 wagging
f_{10}	0.9959	$R_{23}-R_{27}$	phenyl C−H wagging
f_{11}	0.9185	$R_{31}-R_{33}$	ring puckering motions

[a] Optimized to yield a good overall assignment for the C−H stretching region by assigning only the few most intense C−H vibrations. This factor was then kept fixed during the entire subsequent scaling procedure. [b] Optimization was started with a factor of 0.79.

TABLE 9: Frequencies and Intensities of IR Transition of 1-h_6 Calculated on the Basis of the SQM Force Field of 1 Obtained from a Fit over the IR Spectra of Three Isotopomers[a]

no.	sym	SQM	exp.	diff.	% int.	potential energy distribution[b]
1	**A′**	3116.3			5.9	8(99)
2		3080.0			26.4	13(38) + 10/12(23) + 11(11)
3		3072.9	3073	−0.1	64.1	10(52) + 13/11(15) + 9(12)
4		3066.8			34.8	9(54) + 13(25) + 11(9)
5		3055.0	3060	not found	6.8	12(55) + 11(15) + 10/9(12)
6		3048.6	3035	not found	5.7	11(49) + 9/13(17) + 12(14)
7		1566.7	1562	4.7	0.9	6(25) + 3(22) + 18(10)
8		1540.4	1538	2.4	2.8	5(22) + 20(19) + 4(16)
9		1461.5	1458	3.5	9.9	16(24) + 17(20) + 19/7(11)
10		1428.8	1428	0.8	7.0	18(22) + 6/19(16) + 3/20(13)
11		1319.8	1325	−5.2	0.2	16(23) + 17(20) + 20(14) + 3(10)
12		1292.5	1290	2.5	0.3	1(63) + 28(12)
13		1270.2	1264	6.2	2.7	2(26) + 7(21)
14		1161.3	1160	1.3	0.5	16/18(18) + 17(16) + 19(13)
15		1150.8	1149	1.8	0.2	20(33) + 19(22) + 18(18)
16		1079.4	1091	−11.6	4.9	6(14) + 3/120(13) + 4/16/17(11)
17		1012.5	1017	−4.5	3.4	5(32) + 4(30)
18		974.7	976	−1.3	1.1	28(64)
19		842.8	840	2.8	22.2	14(36) + 2(26) + 1/21(10)
20		792.1	788	4.1	15.1	14(53) + 7(24)
21		617.7	612	5.7	0.3	30(85)
22		528.1	525	3.1	0.2	29(79)
23		347.1	343	4.1	6.2	15(77) + 14(15)
24	**A″**	970.1			0.1	26(26) + 31(24) + 25/27(16)
25		946.0			0.0	25/33(28) + 26(18) + 23/24(12)
26		885.7	884	1.7	6.4	27(35) + 24(23) + 23(20) + 32(16)
27		829.3	835	−5.7	0.0	23(37) + 24(30) + 26(16) + 25(14)
28		747.3	741	6.3	100.0	27(37) + 22(17) + 23(15) + 24(12)
29		668.5	670	−1.5	27.0	31(48) + 25/26(18) + 22(16)
30		498.0	497	1.0	11.1	21(54) + 22(29)
31		445.0	443	2.0	42.6	21(46) + 22(25) + 32(16)
32		392.7	392	0.7	0.5	33(72)
33		199.2			1.4	32(57) + 31(15) + 22(13)

[a] The force fields for the d_6 and the d_1-isotopomers, together with the spectra on which they are based, are given in the Supporting Information. [b] Composition of normal modes in terms of the valence (=symmetry) coordinates R_1-R_{33} in Table 7 (% contribution in parentheses; only coordinates that contribute >10% are listed). Components spearated by a slash make the same contribution within 2%.

discrepancy between calculation and experiment with regard to the intensity of ν_{19} and ν_{20} may indicate that B3LYP does not model this redistribution correctly.

4. Conclusion

The full UV/VIS and IR spectra of phenylmethylene (**1**) and its rearrangement product, cycloheptatetraene (**2**), were obtained by observing the spectral changes on >420 nm bleaching of pure samples of **1** (obtained from PDM by laser irradiation at 480−520 nm) as well as **1**-d_1 and **1**-d_6. The optical spectrum of **1** is very reminiscent of that of the benzyl radical **2** which, in view of the fact that the two compounds are iso-π-electronic, is perhaps not surprising. However, it shows that the unpaired in-plane electron does not interfere noticeably with the benzyl-type π-electronic structure of triplet **1**. This electronic structure can be explained readily in terms of four excited configurations that undergo pairwise mixing. This picture is quantified by means of CASPT2 excited-state calculations.

The IR spectrum of **2** can be readily assigned on the basis of B3LYP calculations. Optimization of the corresponding force field according to the method of Pulay et al.[21] results in only minor improvement of the agreement with experiment, but it results in a full description of the normal modes in terms of valence coordinates. In the case of **1**, the assignment of the vibrational spectrum is less straightforward because of pronounced anharmonicity of the Ph−C−H bending deformation. Separate scaling of this mode leads to a better agreement with the experimental spectrum, but the intensities of the vibrations involving this deformation are still predicted much too high, presumably due to a fault in the underlying B3LYP model.

Acknowledgment. This project is part of object no. 2000-053568.98 of the Swiss National Science Foundation. We are indebted to our colleagues from the carbene community for attracting our attention to this problem. We thank Dr. W. Mohr (University of Bern, Switzerland) for calculating the reduced moments of inertia for the Ph−C−H bending deformation of **1**.

Supporting Information Available: PDF file with three figures (consisting of 3 parts each) showing the complete experimental IR difference spectra for the bleaching of **1**-h_6, **1**-d_1, and **1**-d_6, as well as the SQM calculated spectra for the three isotopomers of **1** and **2**. Six tables listing all observed and calculated IR peaks as well as their assignment in terms of internal coordinates plus a table listing the results of CASPT2 calculations for **2**. This material is available free of charge via the Internet at http://pubs.acs.org.

References and Notes

(1) Trozzolo, A. M.; Murray, R. W.; Wasserman, E. *J. Am. Chem. Soc.* **1962**, *84*, 4990.
(2) See for example, Schaefer, H. F. *Sciene* **1986**, *231*, 1100.
(3) Wassermann, E.; Trozzolo, A. M.; Yager, W. A. *J. Chem. Phys.* **1964**, *40*, 2408.
(4) Joines, R. C.; Turner, A. B.; Jones, W. M. *J. Am. Chem. Soc.* **1969**, *91*, 7754.
(5) Schissel, P.; Kent, M. E.; McAdoo, D. J.; Hedaya, E. *J. Am. Chem. Soc.* **1970**, *92*, 2147.

(6) Wentrup, C.; Wilczek, K. *Helv. Chim. Acta* **1970**, *53*, 1459.
(7) Jones, W. M.; Ennis, C. L. *J. Am. Chem. Soc.* **1969**, *91*, 6391.
(8) Gleiter, R.; Hoffmann, R. *J. Am. Chem. Soc.* **1968**, *90*, 5457.
(9) West, P. R.; Chapman, O. L.; LeRoux, J.-P. *J. Am. Chem. Soc.* **1982**, *104*, 1779.
(10) McMahon, R. J.; Abelt, C. J.; Chapman, O. L.; Johnson, J. W.; Kreil, C. L.; LeRoux, J.-P.; Mooring, A. M.; West, P. L. *J. Am. Chem. Soc.* **1987**, *109*, 2456.
(11) Matzinger, S.; Bally, T.; Patterson, E. V.; McMahon, R. J. *J. Am. Chem. Soc.* **1996**, *118*, 1535.
(12) Schreiner, P. R.; Karney, W. L.; Schleyer, P. v. R.; Borden, W. T.; Hamilton, T. P.; Schaefer, H. E. *J. Org. Chem.* **1996**, *61*, 7030.
(13) Wong, M. W.; Wentrup, C. *J. Org. Chem.* **1996**, *61*, 7022.
(14) Matzinger, S.; Bally, T.; Bednarek, P. Manuscript in preparation.
(15) Creary, X. *Org. Synth.* **1986**, *64*, 207.
(16) Dilthey, W.; Scheidt, P. *J. Prakt. Chem.* **1935**, *142*, 125.
(17) The very efficient broadband photolysis of PDM in the UV does not lead to any quantity of **1** that is detectable by absorption spectroscopy.
(18) Andersson, K.; Roos, B. O. In *Modern Electronic Structure Theory*; World Scientific Publ. Co.: Singapore, 1995; Vol. Part 1, Vol. 2; pp 55.
(19) Pierloot, K.; Dumez, B.; Widmark, P.-O.; Roos, B. O. *Theor. Chim. Acta* **1995**, *90*, 87.
(20) Andersson, K.; Blomberg, M. R. A.; Fülscher, M. P.; Kellö, V.; Lindh, R.; Malmqvist, P.-Å.; Noga, J.; Olson, J.; Roos, B. O.; Sadlej, A.; Siegbahn, P. E. M.; Urban, M.; Widmark, P.-O. MOLCAS, Versions 3 and 4: University of Lund, Sweden, 1994.
(21) Pulay, P.; Fogarasi, G.; Pang, F.; Boggs, J. E. *J. Am. Chem. Soc.* **1979**, *101*, 2550.
(22) Tang, W. Ph.D. Dissertation no. 1017, University of Fribourg, Switzerland, 1992.
(23) Tang, W.; Zhang, X.; Bally, T. *J. Phys. Chem.* **1993**, *97*, 4373−80.
(24) McMahon, R. J., personal communication.
(25) Friedrich, D. M.; Albrecht, A. C. *Chem. Phys.* **1974**, *6*, 366.
(26) A similar analogy between the diphenylmethyl radical and diphenyl carbene has been pointed out previously: Hadel, L. M.; Platz, M. S.; Scaiano, J. C. *J. Am. Chem. Soc.* **1984**, *196*, 283.
(27) Rice, J. E.; Handy, N. C.; Knowles, P. J. *J. Chem. Soc., Faraday Trans. 2* **1987**, *83*, 1643.
(28) All states of **1** and **2** are described correctly within the theoretical framework of this model, that is, the CASPT2 wave functions are described to 74−77% by the CASSCF reference wave functions.
(29) Orlandi, G.; Poggi, G.; Zerbetto, F. *Chem. Phys. Lett.* **1985**, *115*, 253.
(30) Negri, F.; Orlanid, G.; Zerbetto, F.; Zgierski, M. Z. *J. Chem. Phys.* **1990**, *93*, 600.
(31) Bunker, P. R.; Jensen, P. *J. Chem. Phys.* **1983**, *79*, 1224.
(32) Note that the inversion potential of 2130 cm^{-1} from this calculation is close to the 1930 ± 30 cm−1 found for $^3CH_2$ (Bunker, P. R.; Jensen, P.; Kraemer, W. P.; Beardsworth, R. *J. Chem. Phys.* **1986**, *85*, 3724).
(33) The harmonic potential was represented by $V(x) = 0.05296x^2$ and the full anharmonic potential by $V(x) = -0.03400x^2 + 0.00328x^4 - 0.00628x^6$, where V is in hartree and x is the deviation of the angle from the equilibrium value (134°) in radians. A reduced mass of 1.179 amu was calculated from the B3LYP optimized structure after a treatment based on reduced moments of inertia (Mohr, W. University of Bern, Switzerland, private communication).
(34) The rest of the spectrum is only marginally affected by this (see Supporting Information).